Available online at www.sciencedirect.com
ScienceDirect
Chinese Journal of Natural Medicines 2022, **20**(7): 541-550
doi: 10.1016/S1875-5364(22)60165-1
Chinese Journal of Natural Medicines

•Research article•

Antiproliferative piperidine alkaloids from giant taro (*Alocasia macrorrhiza*)

GAO Wei[1], WANG Yi[1], WANG Ru[1], WANG Yi-Hai[1, 2*], XU Jing-Wen[1, 2], HE Xiang-Jiu[1, 2*]

[1] *School of Pharmacy, Guangdong Pharmaceutical University, Guangzhou 510006, China;*
[2] *Guangdong Engineering Research Center for Lead Compounds & Drug Discovery, Guangzhou 510006, China*

Available online 20 Jul., 2022

[ABSTRACT] The rhizome of giant taro (*Alocasia macrorrhiza* (L.) Schott), which is a highly adaptable wild plant, is a traditional Chinese herbal medicine. In the current study, the antiproliferative constituents of giant taro were investigated and six new (**1**−**6**) and four known piperidine alkaloids (**7**−**10**) were isolated from its rhizomes. Their chemical structures and absolute configurations were elucidated using various spectroscopic methods and the Mosher ester method. The isolated alkaloids were screened for the antiproliferative activity through MTT assay. The results indicated that piperidine alkaloids exerted potential antiproliferative activity against HepG2, AGS and MCF-7 tumor cells. Further researches showed that compounds **3**−**5** dose-dependently decreased the colony formation rate and induced the apoptosis of AGS cells, while compound **4** induced AGS cell death *via* the proapoptotic pathway. This study demonstrates that the piperidine alkaloids isolated from giant taro exhibit significant antitumor activity, which provides phytochemical evidence for further development and utilization.

[KEY WORDS] Giant taro; *Alocasia macrorrhiza*; Piperidine alkaloids; Antiproliferative; Apoptosis
[CLC Number] R284, R965 **[Document code]** A **[Article ID]** 2095-6975(2022)07-0541-10

Introduction

Giant taro (*Alocasia macrorrhiza* (L.) Schott) is a perennial evergreen herb of the genus *Alocasia*, which is mainly distributed in China and Southeast Asia [1]. In northeast India, it is used as an indigenous food due to the high levels of carotenoids [2]. In China, it grows rapidly and often used as a garden landscape plant for its graceful appearance. In addition, giant taro has also been reported as poultry feed [3], and their rhizomes are rich in starch and can be used for industrial purposes [4, 5]. However, the most important use of giant taro is to treat high fever, influenza, malaria, and malignant tumors [6] as a traditional Chinese herbal medicine.

Previous studies concerning the bioactivity of the genus *Alocasia* have reported that its ethanol or methanol extract exhibited anticancer [7-9], anti-inflammatory [10], antioxidant [11, 12], antimicrobial [13, 14], antihyperglycemic [11], hepatoprotective [15] and antiviral [14] activities. Phytochemical investigation on the genus *Alocasia* resulted in the identification of indole alkaloids [16, 17], piperidine alkaloids [18], lignanamides [19, 20] and other types of alkaloids [21-25]. In addition, terpenoids, lignans, benzene derivatives, flavonoids, sterols and fatty acids [25, 26] were also isolated from giant taro. The alkaloids from *Alocasia* exhibited significant bioactivities against hepatoma [16], gastric cancer, nasopharyngeal cancer [10, 18] and breast cancer as well as anti-inflammatory effects [10].

Plant-derived natural constituents play an important role in novel drug dicovery [27]. For example, camptothecin, paclitaxel, vinblastine, vincristine, and harringtonine are all isolated from plants and have been used as the first-line anticancer drugs because of their promising antitumor activity. A few literatures have reported that the extract of giant taro has a wide range of antitumor activities, which indicated its poteinal role as a new lead compounds of antitumor drugs. However, the specific components that contribute to the promising bioactivity have not been clarified [7]. According to our previous study, a large number of alkaloid components were present in giant taro, for example indole alkaloids, lignan alkaloids, and piperidine alkaloids from rhizomes. But only piperidine alkaloids exhibited excellent antitumor activity [10, 18]. In search for alkaloids with antitumor activity, the

[Received on] 26-Feb.-2022
[Research funding] This work was supported by the National Natural Science Foundation of China (No. 82173698), the Guangdong Province Universities and Colleges Pearl River Scholar Funded Scheme (2017), and the Pearl River S&T Nova Program of Guangzhou (No. 201806010169).
[*]**Corresponding author]** Tel/Fax: 86-20-3935-2140, E-mail: wangyih88@163.com (WANG Yi-Hai); Tel/Fax: 86-20-3935-2132, E-mail: hexiangjiu@163.com (HE Xiang-Jiu)
These authors have no conflict of interest to declare.

rhizomes of giant taro were investigated. In the current study, the dichloromethane soluble extract of the rhizome of giant taro led to isolation of six new and four known piperidine alkaloids. The structures of the six new compounds (**1**−**6**) were determinted by spectroscopic spectra. The Mosher method was used to determine the absolute configuration of compounds **1**−**6**. Their antiproliferative activity against HepG2, AGS and MCF-7 tumor cell lines and the mechanism of antiproliferative activity against AGS cells were investigated.

Results and Discussion

In this study, the dichloromethane soluble fraction of the 95% ethanol extract of giant taro was separated by silica gel, ODS and Sephadex LH-20 chromatography and purified by semi-preparative HPLC. As a result, six new (**1**−**6**) and four (**7**−**10**) known piperidine alkaloids were obtained. Their structures (Fig. 1) were identified by spectroscopic data and a modified Mosher method. All isolated compounds were evaluated for their antitumor activity.

Compound **1** was obtained as a white crystal (MeOH). The molecular formula was deduced to be $C_{21}H_{35}NO_2$ based on the ion *m/z* 334.2704 $[M + H]^+$ (Calcd. for $C_{21}H_{36}NO_2$, 334.2741) in its HR-ESI-MS. In the ^{1}H NMR spectrum (Table 1), five aromatic hydrogen signals showed at δ_H 7.26 (2H, m), 7.17 (2H, m) and 7.15 (1H, m) were assigned to a monosubstituted aromatic ring. The proton signals showed at δ_H 0.99 (3H, d, J = 6.2 Hz) and δ_H 1.17−1.30 implied that a methyl group and multiple methylene group existed in the structure. The ^{13}C NMR (Table 1) and DEPT spectra indicated 21 carbon resonances, including one monosubstituted benzene ring [δ_C 142.3, 128.3 (× 2), 128.2 (× 2) and 125.6], four methines (δ_C 71.8, 70.2, 62.3 and 57.9), ten methylenes [δ_C 44.1, 35.2, 31.8, 31.1, 29.6, 29.1 (× 2), 28.9, 28.7 and 25.5], and one methyl group (δ_C 18.5). Compared the spectral data with a series of piperidine alkaloids [18] isolated from giant taro, it suggested that **1** was also a piperidine alkaloid. The piperidine ring substitution patterns of these alkaloids were various, due to the different positions of hydroxyl groups. In the ^{1}H-^{1}H COSY spectrum (Fig. 2), the correlations of δ_H 0.99 (3H, d, J = 6.2 Hz, 2-Me)/2.15 (1H, dq, J = 8.5, 6.2 Hz, H-2), H-2/δ_H 2.82 (1H, m, H-3), H-3/δ_H 1.12 (1H, q, J = 11.5 Hz, H-4α), H-4α/δ_H 2.91 (1H, m, H-5), H-5/δ_H 2.07 (1H, td, J = 8.4, 2.5 Hz, H-6), and H-6/δ_H 1.71 (1H, m, H-1′), H-1′/δ_H 1.41 (1H, m, H-2′) established a -$CH_3CHCHCH_2CHCHCH_2CH_2$- fragment. The correlation of δ_H 2.15 (H-2) with δ_C 62.3 (C-6) in HMBC spectrum (Fig. 2) suggested that the presence of a piperidine ring fragment. The correlation of δ_H 0.99 (2-Me) with δ_C 57.9 (C-2), correlations of δ_H 0.99 (2-Me), 2.15 (H-2) with δ_C 71.8 (C-3) and correlation of δ_H 2.07 (H-6) with δ_C 70.2 (C-5) suggested the presence of a fragment of the 2-methyl-3,5-dihydroxy-piperidine ring in compound **1**. Furthermore, the correlations of δ_H 2.07 (H-6) with δ_C 31.8 (C-1′) and 25.5 (C-2′) in the HMBC spectrum indicated that the piperidine ring fragment was linked to fatty chain in **1**.

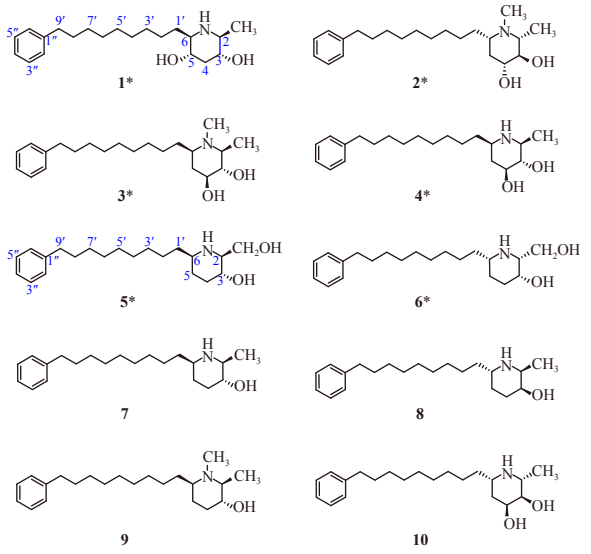

Fig. 1 Structures of compounds separated from giant taro (*: new compound)

In NOESY spectrum (Supporting information, Fig. S10), the correlations from δ_H 2.91 (H-5) to 2.82 (H-3) and 1.71 (H-1′) indicated that they were on the same orientation, while H-6 was on the opposite orientation. The correlation from δ_H 1.12 (H-4a) to 2.15 (H-2) suggested that they were on the same orientation. The absolute configuration of C-3 was determined by the Mosher ester method [28]. Treated with (*S*)-MTPA-Cl and (*R*)-MTPA-Cl, the 3-OH and 5-OH of **1** were esterified to afford the (*S*)- and (*R*)-MTPA ester of **1**, respectively. The absolute configuration of C-3 was determined as *R* (Fig. 3) by the analysis of ^{1}H NMR chemical shift differences ($\Delta\delta_{S-R}$). As the absolute configuration of C-3 were determined, the configurations of the C-2, C-5 and C-6 were determined as 2*S*, 5*S* and 6*R* based on the above NOESY analysis. Based on the above analysis, compound **1** was determined to be (2*S*,3*R*,5*S*,6*R*)-2-methyl-3,5-dihydroxy-6-(9-phenylnonyl) piperidine.

Compound **2** was obtained as a pale-yellow gum. The molecular formula of $C_{22}H_{37}NO_2$ was deduced based on the ion *m/z* 348.2891 $[M + H]^+$ (Calcd. for $C_{22}H_{38}NO_2$, 348.2897) in its HR-ESI-MS. The ^{1}H and ^{13}C NMR spectra (Table 1) were closely comparable to compound **1**, which indicated that compound **2** was also a piperidine alkaloid. The difference was that the ^{1}H NMR spectrum of **2** had an additional methyl signal at δ_H 2.06 (3H, s), and an additional carbon resonance at δ_C 35.4 assigned to the nitrogen methyl carbon signal. The hydroxyl substituted position of the piperidine ring was further determined by ^{1}H-^{1}H COSY and HMBC spectra (Fig. 2). Combined with the analysis of ^{1}H-^{1}H COSY correlations [δ_H 1.06 (3H, d, J = 6.2 Hz, 2-Me)/2.27 (1H, dq, J = 9.7, 6.2 Hz, H-2), H-2/δ_H 2.97 (1H, dd, J = 9.7, 3.1 Hz, H-3), H-3/δ_H 3.73 (1H, q, J = 3.1 Hz, H-4), H-4/δ_H 1.43 (1H, dt, J = 11.4, 2.6 Hz, H-5α), and H-5α/δ_H 2.38 (1H, m, H-6)] and HMBC correlations from δ_H 1.06 (2-Me) to both δ_C 57.8 (C-2) and 72.3

Table 1 NMR spectroscopic data of compounds 1–3 [a] (*J* in Hz)

No.	1		2		3	
	δ_H	δ_C	δ_H	δ_C	δ_H	δ_C
2	2.15 dq (8.5, 6.2)	57.9	2.27 dq (9.7, 6.2)	57.8	1.82 dq (9.0, 6.2)	62.9
3	2.82 m	71.8	2.97 dd (9.7, 3.1)	72.3	2.74 t (9.0)	76.1
4*α*	1.12 q (11.5)	44.1	3.73 q (3.1)	67.0	3.12 m	72.6
4*β*	2.03 m					
5*α*	2.91 m	70.2	1.43 dt (11.4, 2.6)	35.2	1.65 ddd (12.7, 5.0, 2.3)	36.7
5*β*			1.57 ov		1.22 ov	
6	2.07 td (8.4, 2.5)	62.3	2.38 m	55.1	2.02 m	60.4
2-Me	0.99 d (6.2)	18.5	1.06 d (6.2)	16.8	1.09 d (6.2)	16.8
N-Me	-	-	2.06 s	35.4	2.05 s	35.5
1'	1.71 m; 1.07 m	31.8	1.36, m; 1.27, ov	33.2	1.42 ov; 1.34 ov	33.3
2'	1.41 m; 1.21 m	25.5	1.22 ov; 1.15 ov	24.3	1.22 m	24.4
3'	1.26 ov; 1.23 ov	29.6	1.26 ov; 1.23 ov	29.5	1.24 ov; 1.21 ov	29.5
4'	1.26 ov; 1.23 ov	29.1	1.26 ov; 1.23 ov	29.1	1.26 ov; 1.23 ov	29.0
5'	1.26 ov; 1.23 ov	29.1	1.26 ov; 1.23 ov	29.0	1.26 ov; 1.23 ov	29.0
6'	1.26 ov; 1.23 ov	28.9	1.26 ov; 1.23 ov	28.9	1.26 ov; 1.23 ov	28.9
7'	1.26 ov	28.7	1.26 ov; 1.23 ov	28.7	1.26 ov	28.7
8'	1.54 p (6.9)	31.1	1.54 m	31.1	1.55 p (7.0)	31.1
9'	2.55 t (7.6)	35.2	2.55 t (7.5)	35.3	2.55 t (7.6)	35.2
1"	-	142.3	-	142.3	-	142.3
2", 6"	7.17 m	128.2	7.17 m	128.3	7.17 m	128.2
3", 5"	7.26 m	128.3	7.26 m	128.2	7.26 m	128.3
4"	7.15 m	125.6	7.15 m	125.6	7.15 m	125.6
3-OH	4.50 ov	-	4.28 ov	-	4.61 ov	-
4-OH	-	-	4.26 ov	-	4.55 ov	-
5-OH	4.46 ov	-	-	-	-	-

[a] Measured in DMSO-d_6; ov: signals are overlapped

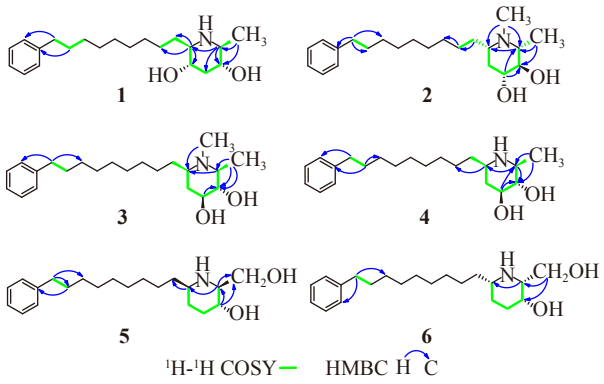

Fig. 2 The selected key ^{1}H-^{1}H COSY and HMBC correlations of compounds 1–6

(C-3), from δ_H 3.73 (H-4) to δ_C 57.8 (C-2) and 72.3 (C-3), from δ_H 2.06 (*N*-Me) to δ_C 57.8 (C-2) and 55.1 (C-6), the presence of *N*,2-dimethyl-3,4-dihydroxy-piperidine ring in **2** was supported. In NOESY spectrum (Supporting information, Fig. S23), the correlations from δ_H 3.73 (H-4) to 2.27 (H-2) and 2.38 (H-6) suggested that these three protons were on the same orientation. The correlation from δ_H 1.43 (H-5a) to 2.97 (H-3) suggested that H-3 and H-5a were on the same orientation. Similarly, the absolute configuration of C-4 was determined as *R* (Fig. 3) according to the Mosher ester method. As the absolute configuration of C-4 was determined, the absolute configurations of C-2, C-3 and C-6 were determined through the above NOESY analysis. Thus, compound **2** was elucidated as (2*R*,3*R*,4*R*,6*S*)-*N*,2-dimethyl-3,4-dihydroxy-6-(9-phenylnonyl) piperidine.

Compound **3** was obtained as a pale-yellow gum. The

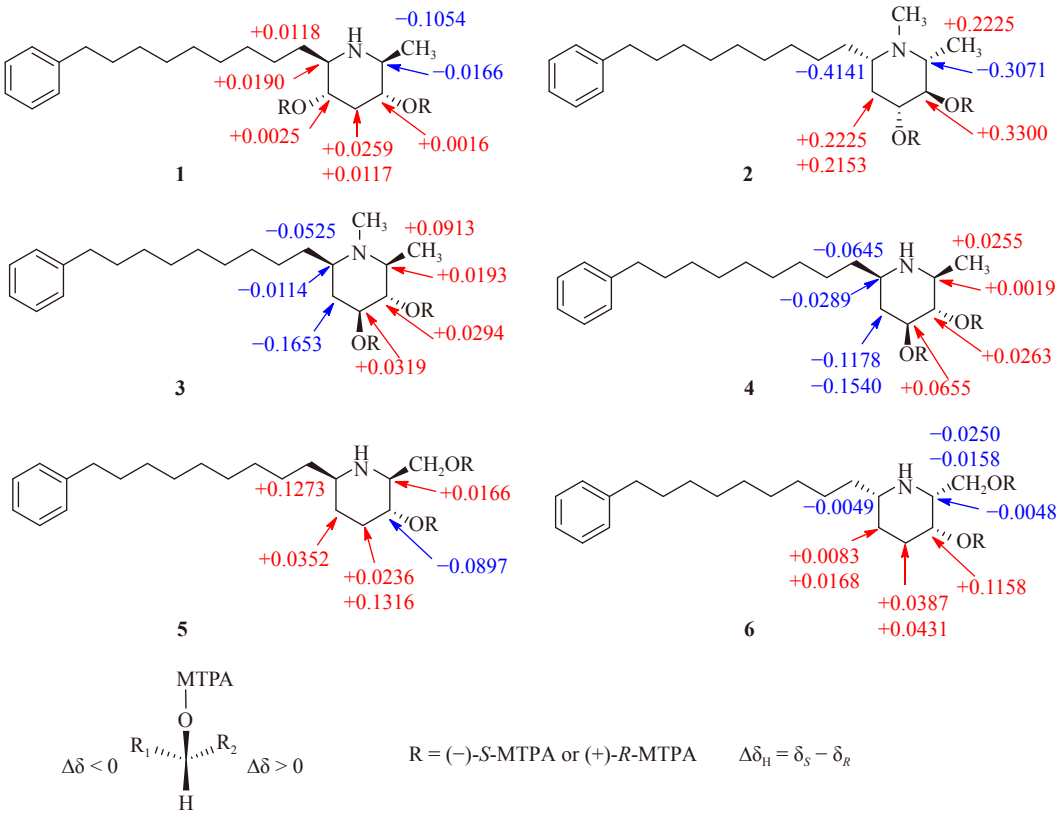

Fig. 3 Values of $\Delta\delta_{S-R}$ of the MTPA esters of compounds 1−6

molecular formula of $C_{22}H_{37}NO_2$ was deduced based on the positive ion *m/z* 348.2891 $[M + H]^+$ (Calcd. for $C_{22}H_{38}NO_2$, 348.2897) in the HR-ESI-MS, indicating that **3** was an isomer of **2**. Compared the ^{13}C NMR spectra (Table 1) of compound **3** with **2**, the main differences lay in the chemical shifts of C-2, C-3, C-4 and C-6 of **3** which appeared downfield about 5 ppm, respectively, suggested that they had different configurations. The observed NOESY (Supporting information, Fig. S36) correlations from δ_H 3.12 (1H, m, H-4) to 1.82 (1H, dq, *J* = 9.0, 6.2 Hz, H-2) and 2.02 (1H, m, H-6) suggested that H-2, H-4 and H-6 were on the same orientation. The correlation from δ_H 1.22 (1H, H-5b) to 2.74 (1H, t, *J* = 9.0 Hz, H-3) suggested that H-3 and H-5b were on the same orientation. The ^1H NMR chemical shift differences of the Mosher ester of **3** were calculated to determined the configuration of C-4 as *S* (Fig. 3). As the absolute configuration of C-4 was determined, the absolute configurations of C-2, C-3 and C-6 were determined through the above NOESY analysis. Based on the above analysis, compound **3** was determined as (2*S*,3*S*,4*S*,6*R*)-*N*,2-dimethyl-3,4-dihydroxy -6-(9-phenylnonyl) piperidine.

Compound **4** was isolated as a white crystal (MeOH), and its molecular formula of $C_{21}H_{35}NO_2$ was obtained by the observed positive ion *m/z* 334.2741 $[M + H]^+$ (Calcd. for $C_{21}H_{36}NO_2$, 334.2741) in the HR-ESI-MS, indicating that **4** was an isomer of **1**. Compared the ^{13}C NMR spectra data (Tables 1 and 2) of compound **4** with **1**, the carbon resonance signals were downfield shifted from δ_C 71.8 (C-3), 70.2 (C-5) and 31.8 (C-1') in **1** to δ_C 78.9 (C-3), 73.1 (C-4) and 36.1 (C-1') in **4**, and upfield shifted from δ_C 62.3, 57.9 and 44.1 in **1** to 55.6, 53.9 and 40.5 in **4**, suggesting that **4** also possessed a dihydroxy substituted piperidine ring. Considering the HMBC correlations (Fig. 2) from δ_H 1.02 (3H, d, *J* = 6.2 Hz, 2-Me) to δ_C 55.6 (C-2) and 78.9 (C-3), from δ_H 2.27 (1H, dq, *J* = 8.9, 6.2 Hz, H-2) to δ_C 78.9 (C-3) and from δ_H 3.14 (1H, m, H-4) to δ_C 55.6 (C-2) and 78.9 (C-3), the presence of a fragment of the 2-methyl-3,4-dihydroxy-piperidine ring in compound **4** was deduced. The NOESY correlations from δ_H 3.14 (H-4) to 2.27 (1H, dq, *J* = 8.9, 6.2 Hz, H-2) and 2.41 (1H, m, H-6) (Supporting information, Fig. S49) indicated that these three protons were on the same orientation. The correlation from δ_H 0.93 (1H, q, *J* = 11.9 Hz, H-5b) to 2.60 (1H, t, *J* = 8.9 Hz, H-3) indicated that H-3 and H-5b were on the same orientation. In addition, the absolute configuration of C-4 was determined as *S* through the Mosher method (Fig. 3). As the absolute configuration of C-4 was determined, the absolute configurations of C-2, C-3 and C-6 were determined through the above NOESY analysis. Therefore, compound **4** was determined as (2*S*,3*S*,4*S*,6*R*)-2-methyl-3,4-dihydroxy-6-(9-phenylnonyl) piperidine.

Compound **5** was obtained as a white plumulaceous crystal (MeOH), and a molecular formula of $C_{21}H_{35}NO_2$ was drawn through its ion peak *m/z* 334.2741 $[M + H]^+$ (Calcd. for $C_{21}H_{36}NO_2$, 334.2741). By the comparison of the ^1H NMR

Table 2 NMR spectroscopic data of compounds 4−6[a] (*J* in Hz)

No.	4		5		6	
	δ_H	δ_C	δ_H	δ_C	δ_H	δ_C
2	2.27 dq (8.9, 6.2)	55.6	2.27 td (8.5, 3.1)	64.4	2.52 ov	61.4
3	2.60 t (8.9)	78.9	2.98 m	68.5	3.59 m	63.3
4*α*	3.14 m	73.1	1.18 m	34.2	1.70 dq (13.3, 2.9)	31.7
4*β*			1.82 dq (11.9, 3.6)		1.42 tdd (13.3, 4.5, 2.1)	
5*α*	1.74 ddd (11.9, 4.5, 1.7)	40.5	1.54 ov	31.4	1.27 ov	26.3
5*β*	0.93 q (11.9)		0.96 m		1.32 ov	
6	2.41 m	53.9	2.33 m	55.4	2.40 m	56.0
2-Me	1.02 d (6.2)	18.8	-	-	-	-
2-CH_2OH	-	-	3.73 dd (10.4, 3.1)	62.9	3.38 ov	62.5
			3.23 dd (10.4, 8.0)		3.33 ov	
1'	1.22 ov	36.1	1.23 ov	36.4	1.28 ov	36.4
2'	1.26 ov; 1.23 ov	25.6	1.23 ov	25.7	1.27 ov; 1.24 ov	25.3
3'	1.26 ov; 1.23 ov	29.4	1.24 ov	29.4	1.27 ov; 1.24 ov	29.2
4'	1.26 ov; 1.23 ov	29.1	1.24 ov	29.1	1.27 ov; 1.24 ov	29.0
5'	1.26 ov; 1.23 ov	29.0	1.24 ov	29.0	1.27 ov; 1.24 ov	28.9
6'	1.26 ov; 1.23 ov	28.9	1.24 ov	28.9	1.27 ov; 1.24 ov	28.8
7'	1.25 ov	28.7	1.27 ov	28.7	1.25 ov	28.6
8'	1.54 p (6.9)	31.1	1.54 ov	31.1	1.54 p (7.5)	31.0
9'	2.55 t (7.6)	35.2	2.55 t (7.6)	35.2	2.55 t (7.5)	35.1
1''	-	142.3	-	142.3	-	142.3
2'', 6''	7.17 m	128.2	7.17 m	128.2	7.17 m	128.19
3'', 5''	7.26 m	128.3	7.26 m	128.3	7.26 m	128.23
4''	7.15 m	125.6	7.15 m	125.6	7.15 m	125.6
2-CH_2OH	-	-	4.50 s	-	4.48 s	-
3-OH	4.50 s	-	4.50 s	-	4.01 s	-
4-OH	4.50 s	-	-	-	-	-

[a] Measured in DMSO-d_6; ov: signals are overlapped

spectra data (Tables 1 and 2) of **1** and **5**, the findings that the methyl signal at δ_C 18.5 (2-Me) of **1** disappeared in **5**, presumed that the 2-Me was substituted. In the ^{13}C NMR and DEPT spectra, the secondary carbon resonance signal was at δ_C 62.9, suggested that C-2-Me was linked to a hydroxymethyl group. From the analysis of ^1H-^1H COSY correlations [δ_H 3.73 (1H, dd, J = 10.4, 3.1 Hz, 2-CH_2OH)/2.27 (1H, td, J = 8.5, 3.1 Hz, H-2), H-2/δ_H 2.98 (1H, m, H-3), H-3/δ_H 1.82 (1H, dq, J = 11.9, 3.6 Hz, H-4*β*), H-4*β*/δ_H 1.54 (1H, ov, H-5*α*) and H-5*α*/δ_H 2.33 (H-6)], as well as the HMBC correlations (Fig. 2) from [δ_H 2.27 (H-2) to δ_C 55.4 (C-6), from δ_H 2.98 (H-3) to δ_C 64.4 (C-2) and 62.9 (2-CH_2OH)], a 2-hydroxymethyl-3-hydroxy-piperidine ring was deduced to exist in **5**. In the NOESY spectum, the correlations (Supporting information, Fig. S62) from δ_H 2.98 (H-3) to 0.96 (H-5), from H-5 to 1.23 (H-1′), suggested that H-3 and H-6 were on the opposite orientation. The correlation from δ_H 2.33 (H-6) to 2.27 (H-2) suggested that H-2 and H-6 were on the same orientation. Accodingly, the absolute configuration of C-3 was determined as *R*, according to the ^1H NMR chemical shift differences of the Mosher ester. As the absolute configuration of C-3 was determined, the absolute configurations of C-2 and C-6 were determined through the above NOESY analysis. Accordingly, compound **5** was elucidated as (2*S*,3*R*,6*R*)-2-hydroxymethyl-3-hydroxyl-6-(9-phenylnonyl) piperidine.

Compound **6** was obtained as a pale-yellow gum, and possessed the same molecular formula as **5** by its ion peak at *m/z* 334.2741 $[M + H]^+$ (Calcd. for $C_{21}H_{36}NO_2$, 334.2741) in

the HR-ESI-MS. The NMR spectra of **6** were found to be closely comparable to that of **5**, except the carbon signals shifted upfield from δ_C 64.4 (C-2), 68.5 (C-3), 62.9 (2-CH_2OH), 34.2 (C-4) and 31.4 (C-5) in **5** to δ_C 61.4 (C-2), 63.3 (C-3), 62.5 (2-CH_2OH), 31.7 (C-4) and 26.3 (C-5) in **6**, and shifted downfield from δ_C 55.4 (C-6) in **5** to δ_C 56.0 (C-6) in **6**. In the HMBC spectrum (Fig. 2), the correlations from δ_H 3.33 (1H, ov, 2-CH_2OH) to δ_C 61.4 (C-2) and 63.3 (C-3) suggested that a 2-hydroxymethyl-3-hydroxy piperidine ring fragment was in **6**, and indicated that **5** and **6** were a pair of stereo-isomer. Moreover, the NOESY correlations (Supporting information, Fig. S75) from δ_H 3.59 (1H, H-3) to 1.32 (1H, m, H-5), from H-5 to 2.52 (1H, H-2), suggested that H-2 and H-3 were on the same orientation. The correlations from δ_H 2.52 (H-2) to 1.42 (1H, ddd, J = 13.3, 4.5, 2.1, H-4b) and 2.40 (1H, H-6) indicated that H-2 and H-6 were on the same orientation. Accordingly, the absolute configuration of C-3 was established to be *R* based on the Mosher ester model. As the absolute configuration of C-3 was determined, the absolute configurations of C-2 and C-6 were determined through the above NOESY analysis. Finally, compound **6** was determined to be (2*R*,3*R*,6*S*)-2-hydroxymethyl-3-hydroxy-6-(9-phenylnonyl) piperidine.

The four known piperidine alkaloids were identified as (2*S*,3*R*,6*R*)-2-methyl-6-(9-phenylnonyl) piperidin-3-ol (**7**), (2*S*,3*S*,6*S*)-2-methyl-6-(9-phenylnonyl piperidin-3-ol (**8**) [18], (−)-(2*R*,3*S*,6*S*)-*N*,2-dimethyl-3-hydroxy-6-(9-phenylnonyl) piperidine (**9**) [29], and (2*R*,3*R*,4*S*,6*S*)-2-methyl-6-(9-phenylnonyl) piperidine-3,4-diol (**10**) [18] by comparison with literature data.

All isolated alkaloids (**1**−**10**) were evaluated for their antiproliferative activity against HepG2, AGS and MCF-7 human tumor cell lines and Hacat normal cell line by MTT assay. The results demonstrated that all alkaloids showed significant inhibitory activity compared with the positive control (Table 3). As show in Fig. 4A, compounds **3**−**5** showed stronger inhibitory effects against the proliferation of AGS cells.

To explore the mechanism by which compounds **3**−**5** exerted antiproliferative effect on gastric cancer cells, the cell morphology, colony formation, and apoptotic rate were determined in the current study. We first observed cell morphology under an inverted microscope. Fig. 4B showed that after treatment with compounds **3**−**5** for 24 h, the number of AGS cells decreased and the cells became round and afloat. Then, compounds **3**−**5** inhibited the clonogenic number of AGS cells in a concentration dependent manner (Fig. 4C). Hoechst 33258 staining showed that after treatment with compounds **3**−**5**, the nuclei of AGS cells were shrunken and apoptotic bodies appeared (Fig. 4D). To further confirm the presence of apoptosis, the annexin V-FITC/PI staining was analyzed by flow cytometry. As shown in Fig. 4E, compounds **3**−**5** significantly increased annexin V-FITC positive cells in a concentration-dependent manner. Moreover, the apoptosis-related proteins were also determined by Western blot after treatment with the most sensitive compound **4** in AGS cells. Fig. 4F showed that compound **4** significantly increased the levels of pro-apoptotic proteins cleaved-PARP-1 and cleaved-caspase3, but decreased the levels of anti-apoptotic proteins Bcl-2. Taken together, the results demonstrated that compounds **1**−**10** have potential anti-proliferative activity against HepG2, AGS and MCF-7 cells, while piperidine alkaloids induced the death of gastric cancer cells through apoptosis pathway.

Table 3 The antiproliferative activity of alkaloids from giant taro against tumor and normal cells (means ± SD, n = 3)

Compd	IC_{50}/(μmol·L^{-1})			
	HepG2	AGS	MCF-7	Hacat
1	12.14 ± 0.26*	18.16 ± 0.63**	30.19 ± 1.12***	21.40 ± 0.93
2	13.65 ± 1.31**	12.11 ± 1.31	47.08 ± 5.33****	20.35 ± 3.13
3	15.17 ± 0.35***	14.38 ± 0.33	31.20 ± 1.18****	21.16 ± 3.51
4	7.20 ± 0.23	9.38 ± 0.27	17.31 ± 4.49*	13.80 ± 0.52
5	11.05 ± 0.13	11.34 ± 0.45	30.93 ± 5.07****	15.47 ± 2.40
6	9.61 ± 0.21***	10.83 ± 0.17	27.46 ± 2.13****	18.19 ± 1.32
7	8.59 ± 0.09	9.54 ± 0.43*	18.95 ± 0.72**	10.49 ± 0.70*
8	9.22 ± 0.13**	8.77 ± 0.45***	23.97 ± 0.65****	18.10 ± 2.84
9	10.47 ± 0.16****	12.20 ± 0.43	24.66 ± 0.39****	18.25 ± 3.75
10	6.68 ± 1.33	8.14 ± 0.59****	14.73 ± 4.07	12.46 ± 1.53
Cisp.[b]	6.93 ± 0.96	11.39 ± 1.22	11.45 ± 1.98	17.10 ± 1.35

$^{*}P < 0.05$, $^{**}P < 0.01$, $^{***}P < 0.001$, $^{****}P < 0.0001$ *vs* control group;
[b] Positive control

Experimental

Instruments and chemicals

NMR spectra were obtained on an Avance III-400, III-500 (Bruker Inc, Falanden, Switzerland) with TMS as an internal standard. IR spectra were recorded on a PerkinElmer 100 (Waltham, MA, USA) with KBr pellets. HR-ESI-MS spectra were achieved on a Waters ACQUITY UPLC/Xevo G2-XS QTOF (Milford, MA, USA). Preparative HPLC was performed using a Shimadzu HPLC (Kyoto, Japan), consisting of an LC-20AR pump and SPD-20A UV/Visible detector. A semi-preparative column (COSMOSIL, 5C_{18}-MS-II, 10 mm ID × 250 mm, Nacalai Tesque, Kyoto, Japan) was used for HPLC preparation. Silica gel (Anhui Liangchen Silicon Source Material Co., Ltd., Lu'an, China) for open column chromatography, Sephadex LH-20 (GE Healthcare Bio-Sciences, Pittsburgh, PA, USA) and ODS (40−60 μm, Merk KGaA, Darmstadt, Germany) were used for purification. A fluorescence microscope (Zeiss GmbH, Jena, Germany) was used to observe the nuclear morphology. CytoFLEXl flow cytometer was purchased from Beckman Coulter (Brea, CA, USA).

Plant material

The rhizomes of giant taro were collected from Guangzhou Higher Education Mega Center, Guangzhou, China, in

April 2018. The plant materials were identified by Prof. HE Xiang-Jiu (Guangdong Pharmaceutical University, Guangzhou, China). The voucher specimen (No. GDPU-NPR-20140811) was deposited at the Lead Compounds Lab, Guangdong Pharmaceutical University, Guangzhou, China.

Extraction and isolation

The sliced fresh rhizomes of giant taro (250 kg) were refluxed with 100 L 95% EtOH for four times, and each for 4 h. The EtOH extract was distilled under reduced pressure at 70 °C to remove alcohol, obtaining a 15 L concentrated suspension. Then, the suspension was extracted with CH_2Cl_2, EtOAc, and *n*-BuOH, respectively. The CH_2Cl_2 fraction (260.00 g) was separated through a silica gel column with CH_2Cl_2 : MeOH (100 : 1 to 3 : 1, *V/V*) as gradient elution to get 14 fractions (A-1 to A-14). Fraction A-12 (40.00 g) was subjected to reverse phase MPLC with gradient elution of MeOH : H_2O (10% to 90 %, *V/V*) to yield 8 subfractions (A-12-1 to A-12-8). Five subfractions (A-12-8-1 to A-12-8-5) were obtained through the separation of fraction A12-8 (28.00 g) using a silica gel column with CH_2Cl_2 : MeOH (70 : 1 to 5 : 1, *V/V*) as gradient elution.

Subfraction A-12-8-4 (8.09 g) was eluted with MeOH : H_2O (65% to 95%, *V/V*) through ODS MPLC, and then a total of 9 subfractions (A-12-8-4-1 to A-12-8-4-9) were obtained. Fraction A-12-8-4-1 (302.0 mg) was futher purified by preparative HPLC (MeOH : H_2O : TEA, 77 : 23 : 0.05, 3.0 mL·min^{-1}), obtaining subfractions A-12-8-4-1-1, A-12-8-4-1-2 and **7** (134.8 mg, t_R 40.3 min). Fraction A-12-8-4-1-1 (21.5 mg) was purified by preparative HPLC (MeOH : H_2O : TEA, 79 : 21 : 0.05, 3.0 mL·min^{-1}) to yield **5** (8.2 mg, t_R 28.6 min), and **6** (4.2 mg, t_R 30.2 min). Compounds **8** (13.9 mg, t_R 37.9 min) and **9** (22.6 mg, t_R 43.1 min) were isolated from fraction A-12-8-4-1-2 (29.0 mg) by preparative HPLC (MeOH : H_2O : TEA, 81 : 19 : 0.05, 3.0 mL·min^{-1}). Subfraction A-12-8-4-2 was separated by Sephadex LH-20 using CH_2Cl_2 : MeOH (2 : 1, *V/V*) as elution, and then three subfractions (A-12-8-4-2-1 to A-12-8-4-2-3) were collected. Subfraction A-12-8-4-2-1 (79.2 mg) was subjected to preparative HPLC (MeOH : H_2O : TEA, 77 : 23 : 0.05, 3.0 mL·min^{-1}) to afford **1** (8.4 mg, t_R 19.5 min). Subfraction A-12-8-4-3 was futher separated by a silica gel column with CH_2Cl_2 : MeOH (30 : 1 to 2 : 1, *V/V*) as elution to yield five subfractions (A-12-8-4-3-1 to A-12-8-4-3-5). Compounds **2** (11.9 mg, t_R 28.5 min) and **3** (7.9 mg, t_R 26.4 min) were then afforded through the separation of fraction A-12-8-4-3-3 (43.4 mg) by preparative HPLC (MeOH : H_2O : TEA, 69 : 31 : 0.05, 3.0 mL·min^{-1}).

Fraction A-12-8-5 (7.00 g) was separated using MPLC with MeOH : H_2O (60% to 95%, *V/V*) as gradient elution to yield ten subfractions (A-12-8-5-1 to A-12-8-5-10). Compounds **4** (18.1 mg, t_R 22.2 min) and **10** (24.9 mg, t_R 25.7 min) were then purified from fraction A-12-8-5-2 (113.1 mg) by preparative HPLC (MeOH : H_2O : TEA, 69 : 31 : 0.05, 3.0

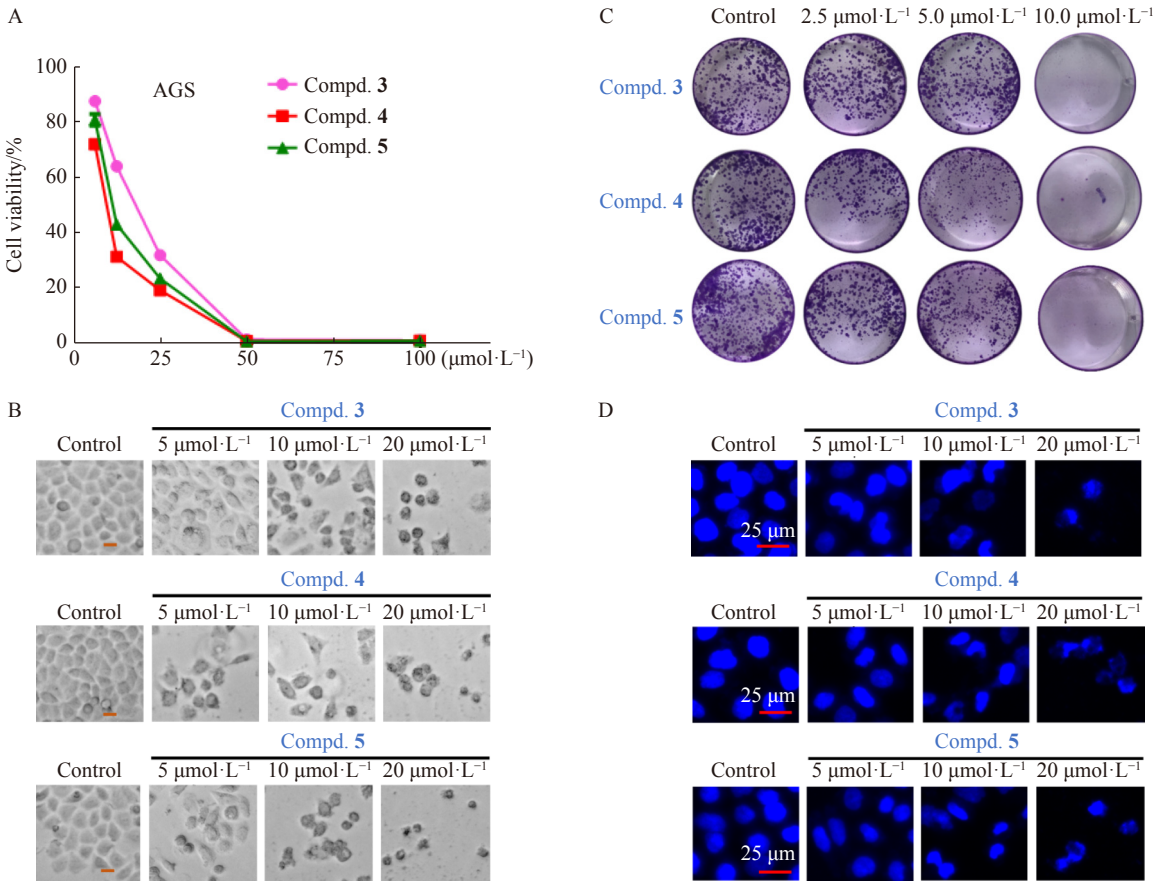

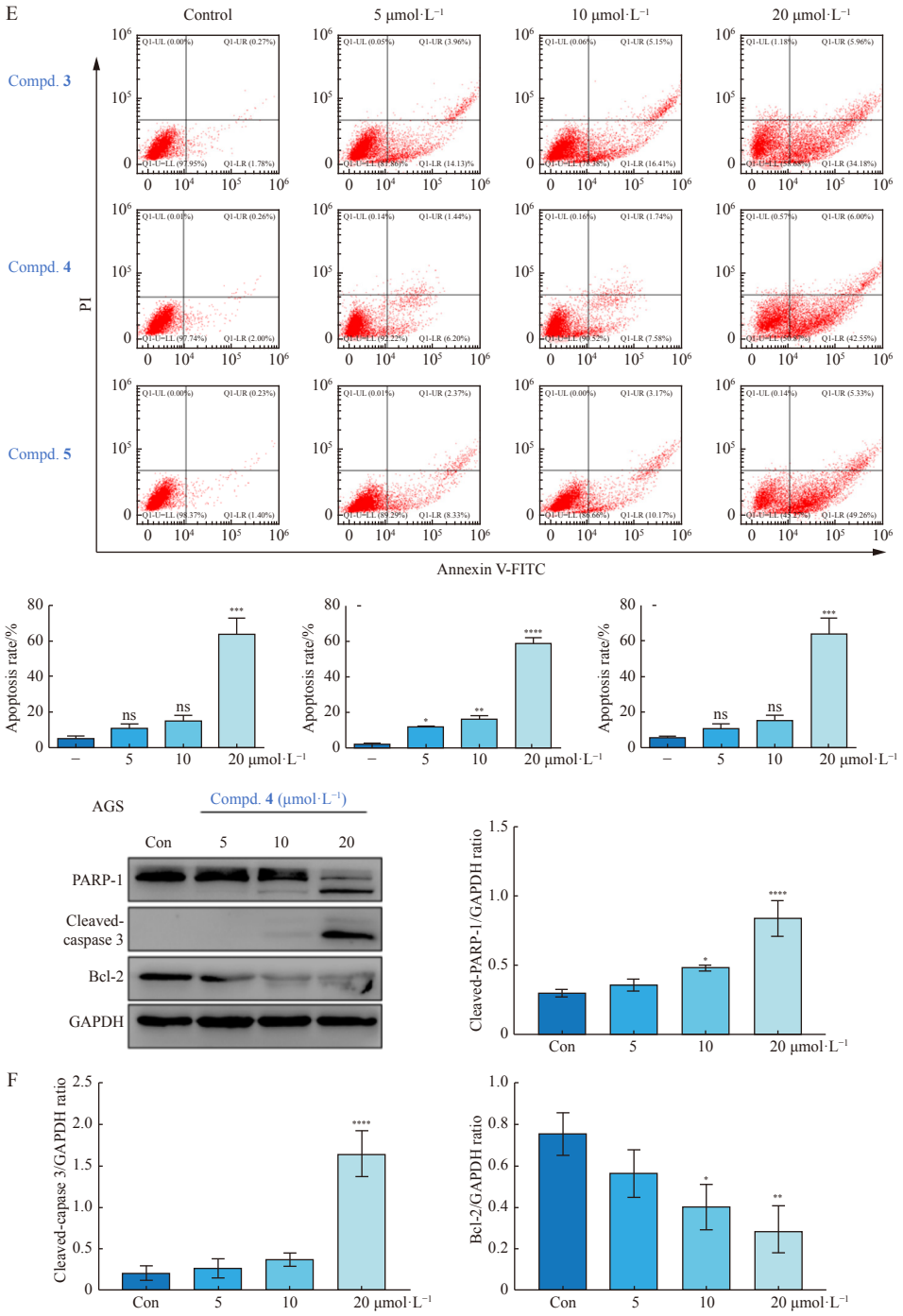

Fig. 4 Compounds 3–5 inhibited the cell viability and induced the apoptosis of AGS cells. (A) AGS cells were treated with different concentrations of compound 3–5 for 48 h and the viability of AGS cells was tested by MTT assay. (B) Changes in cell morphology after treatment with compounds 3–5 . After AGS cells were treated with 5, 10 and 20 μmol·L^{-1} of compounds 3–5 for 48 h, the cell morphology was observed under an inverted microscope. (C) Effects of compounds 3–5 on the proliferation of AGS cells by colony formation assay. The cells were treated with compounds 3–5 at 2.5, 5 and 10 μmol·L^{-1} for 24 h. Then, fresh medium was used to culture for 10 days and the formed colonies were stained with crystal violet. (D) AGS cells were treated with 5, 10 and 20 μmol·L^{-1} of compounds 3–5 for 48 h. Then, the cells were stained with Hoechst 33258 and the nucleus was observed under a fluorescence microscope (scale = 25 μm). (E) Effect of compounds 3–5 on the apoptotic rate of AGS cells. The cells were treated with 5, 10 and 20 μmol·L^{-1} of compounds 3–5 for 24 h, and the number of apoptotic cells was analyzed by flow cytometry. The percentage of apoptotic cells significantly increased. Data were analyzed with GraphPad prism 7.0 and are presented as mean ± SD (n = 3). $^{*}P < 0.05$, $^{**}P < 0.01$, $^{***}P < 0.001$, $^{****}P < 0.0001$ *vs* control group. (F) AGS cells were treated with different concentrations of compound 4 for 24 h and the levels of PARP-1, cleaved-caspase 3 and Bcl-2 were analyzed by Western blot

mL·min^{-1}). See supporting information Fig. S1 for separation scheme.

(2S,3R,5S,6R)-2-methyl-3,5-dihydroxy-6-(9-phenylnonyl) piperidine (**1**): White crystal (MeOH); −3.93° (*c* 0.28, MeOH); IR ν_{max}: 3387, 3265, 2924, 2853, 1456, 1027, 1039, 697 cm^{-1}; NMR data (Table 1); HR-ESI-MS *m/z* 334.2704 $[M + H]^+$ (Calcd. for $C_{21}H_{36}NO_2$, 334.2741).

(2R,3R,4R,6S)-N,2-dimethyl-3,4-dihydroxy-6-(9-phenylnonyl) piperidine (**2**): Pale yellow gum; −29.96° (*c* 0.93, MeOH); IR ν_{max}: 3398, 1455, 1074, 746, 723, 710 cm^{-1}; NMR data (Table 1); HR-ESI-MS *m/z* 348.2891 $[M + H]^+$ (Calcd. for $C_{22}H_{38}NO_2$, 348.2897).

(2S,3S,4S,6R)-N,2-dimethyl-3,4-dihydroxy-6-(9-phenylnonyl) piperidine (**3**): Pale yellow gum; +19.15° (*c* 0.26, MeOH); IR ν_{max}: 3377, 2927, 2854, 1455, 1087, 746, 698 cm^{-1}; NMR data (Table 1); HR-ESI-MS *m/z* 348.2891 $[M + H]^+$ (Calcd. for $C_{22}H_{38}NO_2$, 348.2897).

(2S,3S,4S,6R)-2-methyl-3,4-dihydroxy-6-(9-phenylnonyl) piperidine (**4**): White crystal (MeOH); +4.97° (*c* 0.6, MeOH); IR ν_{max}: 3391, 2926, 2854, 1454, 1067, 747, 723, 698 cm^{-1}; NMR data (Table 2); HR-ESI-MS *m/z* 334.2741 $[M + H]^+$ (Calcd. for $C_{21}H_{36}NO_2$, 334.2741).

(2S,3R,6R)-2-hydroxymethyl-3-hydroxy-6-(9-phenylnonyl) piperidine (**5**): White plumulaceous crystal (MeOH); +9.77° (*c* 0.43, MeOH); IR ν_{max} (KBr) cm^{-1}: 3305, 2926, 2854, 1454, 1057, 746, 698; NMR data (Table 2); HR-ESI-MS *m/z* 334.2741 $[M + H]^+$ (Calcd. for $C_{21}H_{36}NO_2$, 334.2741).

(2R,3R,6S)-2-hydroxymethyl-3-hydroxy-6-(9-phenylnonyl) piperidine (**6**): Pale yellow gum; −0.57° (*c* 0.14, MeOH); IR ν_{max} (KBr) cm^{-1}: 3386, 2926, 2854, 1454, 747, 698; NMR data (Table 2); HR-ESI-MS *m/z* 334.2741 $[M + H]^+$ (Calcd. for $C_{21}H_{36}NO_2$, 334.2741).

Preparation of the (S)- and (R)-α-methoxy-α-trifluoromethylphenylacetyl (MTPA) ester derivatives of compounds 1−6

In the current study, the absolute configuration of hydroxyl linked to the piperidine ring was determined by the Mosher method as previously reported [28]. Briefly, the hydroxyl linked to the piperidine ring reacted with (*S*)-MTPA-Cl and (*R*)-MTPA-Cl to afford (*S*) and (*R*)-Mosher esters, respectively. Then, the chemical shifts of the hydrogen signals on the piperidine ring were different due to the different orientation of the benzene ring. Therefore, the absolute configuration of the -OH was determined by comparing the differences in the protons of the (*S*) and (*R*)-Mosher esters ($\Delta\delta_{S-R}$, $\Delta\delta < 0$ were placed to the left of the model and $\Delta\delta > 0$ were placed to the right of the model).

The (*S*)- and (*R*)-MTPA ester of compounds **1**−**6** were obtained according to previous reports [30]. In brief, compounds **1** (1.05 mg, 1.16 mg), **2** (1.5 mg, 1.6 mg), **3** (1.26 mg, 1.21 mg), **4** (1.57 mg, 1.60 mg), **5** (1.17 mg, 1.26 mg), and **6** (1.3 mg, 1.3 mg) were added into the NMR tubes, respectively, and completely dried under vacuum. Then, under a N_2 flow, each NMR tube was added with pyridine-d_5 (each 0.5 mL), (*S*)-(+)-MTPA chloride or (*R*)-(−)-MTPA chloride (each 8 μL), and quickly sealed and shaken. The (*S*)- and (*R*)-MTPA esters were obtained after reaction overnight. The ^{1}H NMR (500 MHz in $CDCl_3$) and ^{1}H-^{1}H COSY spectra of compounds **1**−**6** were recorded and assigned for $\Delta\delta_{S-R}$ calculations (Supporting Information).

Cytotoxicity assay

All isolated alkaloids were evaluated for their antiproliferative activity against HepG2, AGS, MCF-7, and Hacat cell lines by MTT assay. In brief, 5.0×10^3 cells/well were seeded in 96 well plates at 37 °C for 12 h. Then, the different concentrations (6.25, 12.5, 25, 50, and 100 μmol·L^{-1}) of compounds (**1**−**10**) were exposed to the cells for 48 h, and the subsequent steps were performed as previously described [31].

Colony formation assay

AGS cells (400 cells/well) were seeded into 12 well plates and cultured for 24 h, before treatment with different concentrations (2.5, 5, 10 μmol·L^{-1}) of compounds **3**−**5** for 48 h. The following steps were performed as previously reported [32].

Cell morphology

AGS cells (1×10^5 per well) were seeded in a 12 well plate and incubated for 24 h. The cells were treated with compounds **3**−**5** at different concentrations (5, 10, and 20 μmol·L^{-1}), and incubated for 48 h. Then, the changes in cell morphology caused by compounds **3**−**5** were observed as previously reported [33]. In addition, the cells were washed three times with PBS and fixed with 4% paraformaldehyde for 20 min, followed by staining with Hoechst 33258 and the nuclear morphology was observed under a fluorescence microscope.

Cell apoptosis analysis

AGS cells were seeded into 6 well plates (1×10^5 per well) before treatment with compounds **3**−**5** (5, 10, and 20 μmol·L^{-1}) for 24 h. The number of apoptotic cells was quantified using an annexin V-FITC/PI apoptosis detection kit, and analyzed by flow cytometry [32].

Western blot

AGS cells were treated with different concentrations of **4**, and then whole cell lysates were separated on 10%−12% SDS polyacrylamide gel electrophoresis and transferred to PVDF membrane. The membrane was bound with primary and secondary antibodies, and signals were visualized by an ECL Kit (beyotime, Beijing, China).

Supplementary data

The original spectra of **1**−**10**, including IR, ^{1}H, ^{13}C NMR, 2D NMR, and HR-ESI-MS are provided as supplementary data, and can be re-quested by sending E-mails to the corresponding authors.

References

[1] Chinese Academy of Sciences Flora of China Commission. *Flora of China* [M]. Beijing: Science Press, 1979: 76-78.

[2] Chyne DAL, Ananthan R, Longvah T. Food compositional analysis of indigenous foods consumed by the Khasi of

Meghalaya, North-East India [J]. *J Food Compos Anal*, 2019, **77**: 91-100.
[3] Diarra SS, Oikali C, Rasch IM, *et al*. Giant taro (*Alocasia macrorrhiza*) root meal with or without coconut oil slurry as source of dietary energy for laying hens [J]. *Mala J Anim Sci*, 2016, **19**: 31-38.
[4] Valencia GA, Henao ACA, Zapata RAV. Comparative study and characterization of starches isolated from unconventional tuber sources [J]. *J Polym Eng*, 2012, **32**(8-9): 531-537.
[5] Quintero JA, Cardona CA. Ethanol dehydration by adsorption with starchy and cellulosic materials [J]. *Ind Eng Chem Res*, 2009, **48**(14): 6783-6788.
[6] Zhu LH, Meng LJ, Ye WC, *et al*. Study on chemical constituents of *Alocasia macrorrhiza* [J]. *Lishizhen Med Mater Medica Res*, 2013, **24**: 2859-2860.
[7] Fang ST, Lin CY, Zhang QB, *et al*. Anticancer potential of aqueous extract of *Alocasia macrorrhiza* against hepatic cancer *in vitro* and *in vivo* [J]. *J Ethnopharmacol*, 2012, **141**(3): 947-956.
[8] Fang M, Zhu DQ, Luo CH, *et al*. *In vitro* and *in vivo* anti-malignant melanoma activity of *Alocasia cucullata via* modulation of the phosphatase and tensin homolog/phosphoinositide 3-kinase/AKT pathway [J]. *J Ethnopharmacol*, 2018, **213**: 359-365.
[9] Peng W, Chen ZY, Tang X, *et al*. Antitumor effect and apoptosis induction of *Alocasia cucullata* (Lour.) G. Don in human gastric cancer cells *in vitro* and *in vivo* [J]. *BMC Complement Altern Med*, 2015, **15**: 33.
[10] Huang WJ, Li C, Wang YH, *et al*. Anti-inflammatory lignanamides and monoindoles from *Alocasia macrorrhiza* [J]. *Fitoterapia*, 2017, **117**: 126-132.
[11] Rahman MM, Hossain MA, Siddique SA, *et al*. Antihyperglycemic, antioxidant, and cytotoxic activities of *Alocasia macrorrhizos* (L.) rhizome extract [J]. *Turk J Biol*, 2012, **36**: 574-579.
[12] Mandal P, Misra TK, Singh ID. Antioxidant activity in the extracts of two edible aroids [J]. *Indian J Pharm Sci*, 2010, **72**(1): 105-108.
[13] Banik S, Ibrahim M, Amin MN, *et al*. Determination of biological properties of *Alocasia macrorrhizos*: a medicinal plant [J]. *World J Pharm Res*, 2014, **3**(9): 193-210.
[14] Wang HX, Ng TB. Alocasin, an anti-fungal protein from rhizomes of the giant taro *Alocasia macrorrhiza* [J]. *Protein Expr Purif*, 2003, **28**(1): 9-14.
[15] Patil BR, Bamane SH, Khadsare UR. *In vitro* protection of hepatocytes by *Alocasia macrorrhiza* leaf juice against CCl_4 and Tylenol mediated hepatic injury [J]. *Int J Pharm Appl*, 2011, **2**: 122-127.
[16] Zhu LH, Chen C, Wang H, *et al*. Indole alkaloids from *Alocasia macrorrhiza* [J]. *Chem Pharm Bull*, 2012, **60**(5): 670-673.
[17] Elsbaey M, Ahmed KF, Elsebai MF, *et al*. Cytotoxic constituents of *Alocasia macrorrhiza* [J]. *Z Naturforsch C*, 2017, **72**: 21-25.
[18] Huang WJ, Yi XM, Feng JY, *et al*. Piperidine alkaloids from *Alocasia macrorrhiza* [J]. *Phytochemistry*, 2017, **143**: 81-86.
[19] Zhu LH, Huang XS, Ye WC, *et al*. Study on chemical constituents of *Alocasia macrorrhiza* (L.) Schott [J]. *Chin Pharm J*, 2012, **47**: 1029-1031.
[20] Ni Z, Peng W, Liang S, *et al*. Eight phenylpropane lignanamides from the tubers of *Alocasia cucullata* and their cytotoxic and tyrosine kinase inhibitory properties [J]. *Chem Nat Compd*, 2016, **52**: 963-965.
[21] Tien NQ, Ngoc PH, Minh PH, *et al*. New ceramide from *Alocasia macrorrhiza* [J]. *Arch Pharm Res*, 2004, **27**(10): 1020-1022.
[22] Tien NQ, Ngoc PH, Minh PH, *et al*. Two new aloceramides from *Alocasia macrorrhiza* [J]. *J Chem*, 2005, **43**: 513-516.
[23] Nahrstedt A. Cyanogenese der Araceen [J]. *Phytochemistry*, 1975, **14**: 1339-1340.
[24] Kaur A, Kamboj SS, Singh J, *et al*. Isolation of a novel *N*-acetyl-D-lactosamine specific lectin from *Alocasia cucullata* (Schott) [J]. *Biotechnol Lett*, 2005, **27**(22): 1815-1820.
[25] Lei X, Feng Y, Liang S, *et al*. Chemical components of the tuber of *Alocasia cucullata* [J]. *Chem Nat Compd*, 2014, **50**: 133-134.
[26] Peng W, Liang S, Hu J, *et al*. The cytotoxic and tyrosine kinase inhibitory properties of C-21 steroids and iridoids from the tubers of *Alocasia cucullata* [J]. *J Nat Med*, 2016, **70**(3): 602-609.
[27] Newman DJ, Cragg GM. Natural products as sources of new drugs over the nearly four decades from 01/1981 to 09/2019 [J]. *J Nat Prod*, 2020, **83**(3): 770-803.
[28] Li LG, Wang YF, Fu Y, *et al*. Historical story on natural medicinal chemistry: determination of absolute configuration of natural products by Mosher's method [J]. *Chin Tradit Herb Drugs*, 2017, **48**: 225-231.
[29] Zhao FW, Luo M, Wang YH, *et al*. A piperidine alkaloid and limonoids from *Arisaema decipiens*, a traditional antitumor herb used by the Dong people [J]. *Arch Pharm Res*, 2010, **33**(11): 1735-1739.
[30] Still PC, Yi B, Gonzalez-Cestari TF, *et al*. Alkaloids from *Microcos paniculata* with cytotoxic and nicotinic receptor antagonistic activities [J]. *J Nat Prod*, 2013, **76**(2): 243-249.
[31] Yan F, Huang YY, Wang YH, *et al*. Bioactive sterols and triterpenoids from the fruits of giant crepe-myrtle [J]. *Ind Crops Prod*, 2019, **130**: 363-370.
[32] Xu JW, Zhang MM, Lin XY, *et al*. A steroidal saponin isolated from *Allium chinense* simultaneously induces apoptosis and autophagy by modulating the PI3K/Akt/mTOR signaling pathway in human gastric adenocarcinoma [J]. *Steroids*, 2020, **161**: 108672.
[33] Sun LL, Wang Z, Wang YH, *et al*. Anti-proliferative and anti-neuroinflammatory eudesmanolides from Wedelia (*Sphagneticola trilobata* (L.) Pruski) [J]. *Fitoterapia*, 2020, **142**: 104452.

Cite this article as: GAO Wei, WANG Yi, WANG Ru, WANG Yi-Hai, XU Jing-Wen, HE Xiang-Jiu. Antiproliferative piperidine alkaloids from giant taro (*Alocasia macrorrhiza*) [J]. *Chin J Nat Med*, 2022, **20**(7): 541-550.